Reconstruction of Bi-Isotropic Material Parameters from Experimental Data

Rikte, Sten; Sauviac, Bruno; Kristensson, Gerhard; Mariotte, Frédéric

1998

CODEN:LUTEDX/(TEAT-7072)/1-22/(1998)

Reconstruction of Bi-Isotropic Material Parameters from Experimental Data

Sten Rikte, Bruno Sauviac,

Gerhard Kristensson, and Frédéric Mariotte

Department of Electroscience
Electromagnetic Theory
Lund Institute of Technology
Sweden

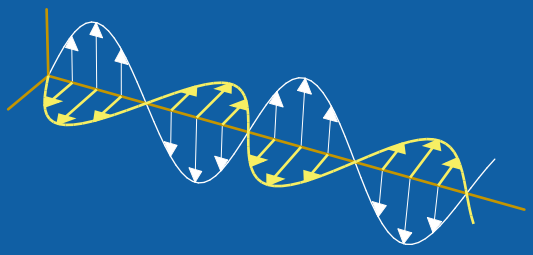

Sten Rikte and Gerhard Kristensson

Department of Electroscience
Electromagnetic Theory
Lund Institute of Technology
P.O. Box 118
SE-221 00 Lund
Sweden

Bruno Sauviac

Laboratoire PIOM - UMR
CNRS 5501
ENSCP—Universite de Bordeaux I
33402 Talence Cedex
France

Frédéric Mariotte

CEA-CESTA
B.P. N°2
33114 Le Barp
France

Editor: Gerhard Kristensson

Abstract

Time-varying wave propagation and time-harmonic wave propagation in bi-isotropic materials are reviewed and the connection between the formulations is established via the temporal Fourier transform. An alternative method to determine the dispersive properties of a bi-isotropic slab from sinusoidal scattering data at normal incidence is presented. A numerical example (realistic, synthetic scattering data) is given to illustrate the theory. Furthermore, experimental data is presented and used to generate the permittivity, permeability, and chirality parameters of a specific man-made chiral slab in the range 3.5–18 GHz. On the basis of the results of inversion, the question whether the passivity concept is too austere is raised.

1 Introduction

In recent years, owing to many potential areas of application, in particular for microwaves and millimeter waves, the interaction of electromagnetic waves and bi-isotropic or isotropic chiral media has attracted much attention. For reviews and references, see, e.g., Engheta and Jaggard [7] or Lakhtakia [13]. Several new books on the subject with the emphasis on microwave applications are also available, see, *e.g.*, Lakhtakia *et al.* [14] and Lindell *et al.* [16], and an electronic forum of discussion (CHIRAL-L) has been established as well.

The characteristic property of the isotropic chiral medium is the chirality, which twists and distorts the plane of polarization of an originally linearly polarized plane wave. In the optical regime, this rotatory effect is known as optical activity, and the epithet electromagnetic activity has been suggested in the general electromagnetic case [14, 16]. The physical origin of electromagnetic activity is resonance phenomena in the handed micro structure of the bi-isotropic medium. Therefore, chirality is believed to be highly dispersive property, *i.e.*, it depends anomalously on frequency.

A linear, homogeneous, isotropic, and temporally dispersive chiral medium is characterized by three time-dependent susceptibility functions. In general, these functions are unknown to the engineer. The present paper concerns the inverse problem of determining the susceptibility functions as functions of frequency in a band at normal incidence.

Inverse problems for bi-isotropic media have been discussed before. Existing experimental techniques are reviewed in [3, 6]. Excellent examples of reconstructions of the susceptibility kernels of both reciprocal and non-reciprocal media on the basis on synthetic scattering data have been reported by Kristensson and Rikte [10, 22]. In these references, time-domain methods have been employed. Frequency-domain methods have been used also. Cloete and Smith [5] have presented an algorithm for the inversion of time-harmonic scattering data at normal incidence using the Weir parameters [27]. More results on time-harmonic measurements using free-space or wave-guide environments and parameter reconstruction can be found in, *e.g.*, [2, 4, 8, 17, 20, 23–26] and in references given therein. In [24], the Kramers–Kronig relations, *i.e.*, causality aspects, were investigated. In the present article, an inverse algorithm close to the one used in [5, 25] is applied to experimental data.

The proposed method does not utilize the propagation factors of the left- and right-hand circularly polarized eigenwaves as in [5]. Instead, the matrix approach in [10, 22] is referred to. Explicitly, the chirality parameter is obtained in the first step of the algorithm from transmission data, whereby the problem essentially is brought back to the isotropic case.

The plan of the present paper is as follows: In Section 2, the direct scattering problem at normal incidence is discussed, both in the time-domain and the frequency-domain. In Section 3, the inverse scattering problem in the frequency-domain is addressed. The proposed inverse algorithm is tested in a numerical example with realistic synthetic scattering data in Section 4. In Section 5, experimental scattering data for a specific man-made isotropic chiral slab is presented and the result of inversion based on this set of data is presented also. The results are discussed in Section 6 and conclusions are drawn in Section 7.

2 Basic equations

In this section, propagation of TEM-waves in linear, homogeneous, isotropic, reciprocal, temporally dispersive, and dissipative chiral slabs is discussed briefly. The steady-state results are well-known, see, for instance, Bassiri *et al.* [1]. A general time-domain analysis, that bears a close resemblance to time-harmonic technique, can be found in Rikte [21]. The connection between the formulations is established by temporal Fourier transformation. In Section 2.1, the basic time-domain results are presented. In Section 2.2, the corresponding time-harmonic results are given.

2.1 Time-domain results

Time is denoted by t and the radius vector by $\boldsymbol{r} = \boldsymbol{e}_x x + \boldsymbol{e}_y y + \boldsymbol{e}_z z$. The two-dimensional dyadics $\mathbf{I} = \boldsymbol{e}_x\boldsymbol{e}_x + \boldsymbol{e}_y\boldsymbol{e}_y$ and $\mathbf{J} = \boldsymbol{e}_z \times \mathbf{I} = \boldsymbol{e}_y\boldsymbol{e}_x - \boldsymbol{e}_x\boldsymbol{e}_y$ are employed also. For simplicity, the slab is assumed to be embedded in vacuum. Medium quantities associated with vacuum are endowed with the subscript 0:

$$\begin{cases} \epsilon_0 = \text{the permittivity of vacuum,} \\ \mu_0 = \text{the permeability of vacuum,} \\ c_0 = 1/\sqrt{\epsilon_0\mu_0} = \text{the speed of light in vacuum,} \\ \eta_0 = \sqrt{\mu_0/\epsilon_0} = \text{the intrinsic impedance of vacuum.} \end{cases}$$

It is well known that a linear, homogeneous, isotropic chiral slab $z \in (0, d)$ supports transverse electric and magnetic (TEM) waves, *i.e.*, solutions to the source-free Maxwell equations

$$\begin{cases} \nabla \times \boldsymbol{E}(\boldsymbol{r}, t) = -\partial_t \boldsymbol{B}(\boldsymbol{r}, t), \\ \nabla \times \boldsymbol{H}(\boldsymbol{r}, t) = \partial_t \boldsymbol{D}(\boldsymbol{r}, t) \end{cases}$$

of the form

$$\begin{cases} \boldsymbol{E}(\boldsymbol{r},t) = \boldsymbol{e}_x E_x(z,t) + \boldsymbol{e}_y E_y(z,t), \\ \boldsymbol{H}(\boldsymbol{r},t) = \boldsymbol{e}_x H_x(z,t) + \boldsymbol{e}_y H_y(z,t). \end{cases}$$

As usual, the electric and magnetic fields at $(\boldsymbol{r},t)$ are denoted by $\boldsymbol{E}(\boldsymbol{r},t)$ and $\boldsymbol{H}(\boldsymbol{r},t)$, respectively, whereas the corresponding flux densities are $\boldsymbol{D}(\boldsymbol{r},t)$ and $\boldsymbol{B}(\boldsymbol{r},t)$. A general scattering relation for the bi-isotropic slab is obtained by considering excitation both from the left and the right. The incident electric fields at the left and right edges are denoted by $\boldsymbol{E}^i_{\text{left}}(t)$ and $\boldsymbol{E}^i_{\text{right}}(t)$, respectively. The corresponding scattered electric fields are denoted by $\boldsymbol{E}^r(t)$ and $\boldsymbol{E}^t(t)$.

In order to solve the Maxwell equations, the constitutive relations of the bi-isotropic medium must be specified. In this paper, the chiral medium is assumed to be linear, homogeneous, isotropic, reciprocal, temporally dispersive, and dissipative; therefore, the pertinent constitutive relations are

$$\begin{cases} \boldsymbol{D}(\boldsymbol{r},t) = \epsilon_r^{\text{opt}}\epsilon_0 \left\{\boldsymbol{E}(\boldsymbol{r},t) + (\chi_e * \boldsymbol{E})(\boldsymbol{r},t)\right\} + c^{-1}(\chi_c * \boldsymbol{H})(\boldsymbol{r},t), \\ \boldsymbol{B}(\boldsymbol{r},t) = -c^{-1}(\chi_c * \boldsymbol{E})(\boldsymbol{r},t) + \mu_r^{\text{opt}}\mu_0 \left\{\boldsymbol{H}(\boldsymbol{r},t) + (\chi_m * \boldsymbol{H})(\boldsymbol{r},t)\right\}, \end{cases}$$

where the asterisk $(*)$ denotes temporal convolution, e.g.,

$$(\chi_e * \boldsymbol{E})(\boldsymbol{r},t) = \int_{-\infty}^{t} \chi_e(t-t')\boldsymbol{E}(\boldsymbol{r},t')\,dt'.$$

For further details, the reader is referred to Karlsson and Kristensson [9].

Observe that several other sets of constitutive relations can be found in the literature, e.g., Post's constitutive relations, where the electric flux density and the magnetic field are expressed in terms of the electric field and the magnetic flux density. Owing to the unique solubility of Volterra equations of the second kind, all these sets of constitutive relations are equivalent, see Kristensson and Rikte [11].

The permittivity and the permeability operators of the medium have both been decomposed in dispersive (memory) and nondispersive (direct) parts. The latter model the fast processes in the material [12]. The former are temporal convolution operators, and generate soft reflections even if the incident fields have finite jump discontinuities. The direct terms cause hard reflections, unless the real number

$$\eta_r^{\text{opt}} := \sqrt{\mu_r^{\text{opt}}/\epsilon_r^{\text{opt}}}$$

equals unity. If equality holds, the medium is said to be optically impedance matched. Because the medium is dissipative and reciprocal, the chirality operator lacks a direct term, see Karlsson and Kristensson [9].

The integral kernels $\chi_e(t)$, $\chi_m(t)$, and $\chi_c(t)$ are the electric susceptibility kernel, the magnetic susceptibility kernel, and the chirality kernel, respectively. Traditionally, the chirality kernel is also denoted by $K(t)$ [11]. Assuming the susceptibility kernels are integrable, the Riemann-Lebesgue lemma implies that

$$\lim_{\omega\to\infty} \int_0^\infty e^{i\omega t}\chi_e(t)\,dt = 0$$

and analogously for $\chi_m(t)$ and $\chi_c(t)$. Accordingly, in the optical limit, the medium becomes achiral with relative permittivity ϵ_r^{opt} and relative permeability μ_r^{opt}. The quantity c present in the constitutive relations is the wave front speed defined by

$$c = c_0/n^{\text{opt}},$$

where the number

$$n^{\text{opt}} := \sqrt{\epsilon_r^{\text{opt}}\mu_r^{\text{opt}}}$$

is interpreted as the index of refraction at high frequencies. Similarly, the quantity η_r^{opt} defined above is interpreted as a relative intrinsic impedance in the optical limit.

The constitutive relations presented above are now slightly manipulated. Specifically, new integral operators representing intrinsic impedance and index of refraction are introduced as

$$\eta(1 + Z*) \quad \text{and} \quad n^{\text{opt}}(1 + N*),$$

respectively, where the optical intrinsic impedance is

$$\eta = \eta_0\eta_r^{\text{opt}}.$$

The integral kernels $N(t)$ and $Z(t)$ are defined as the uniquely determined solutions to the nonlinear Volterra equations

$$\begin{cases} 2N(t) + (N * N)(t) = \chi_e(t) + \chi_m(t) + (\chi_e * \chi_m)(t), \\ 2Z(t) + (Z * Z)(t) = \chi_e^{\text{res}}(t) + \chi_m(t) + (\chi_e^{\text{res}} * \chi_m)(t) \end{cases}$$

of the second kind with inverses

$$\begin{cases} \chi_e(t) = N(t) + Z^{\text{res}}(t) + (Z^{\text{res}} * N)(t), \\ \chi_m(t) = N(t) + Z(t) + (N * Z)(t). \end{cases}$$

The resolvent kernel $\chi_e^{\text{res}}(t)$ of the integral kernel $\chi_e(t)$ is defined as the unique solution to the linear Volterra integral equation of the second kind

$$\chi_e(t) + \chi_e^{\text{res}}(t) + (\chi_e * \chi_e^{\text{res}})(t) = 0$$

and the kernel $Z^{\text{res}}(t)$ is defined analogously. The constitutive relations of the bi-isotropic medium can now be written in the form

$$\begin{cases} \eta(1 + Z*)\boldsymbol{D} = c^{-1}(1 + N*)\boldsymbol{E} + c^{-1}\chi_c * \eta(1 + Z*)\boldsymbol{H}, \\ \boldsymbol{B} = -c^{-1}\chi_c * \boldsymbol{E} + c^{-1}(1 + N*)\eta(1 + Z*)\boldsymbol{H}. \end{cases}$$

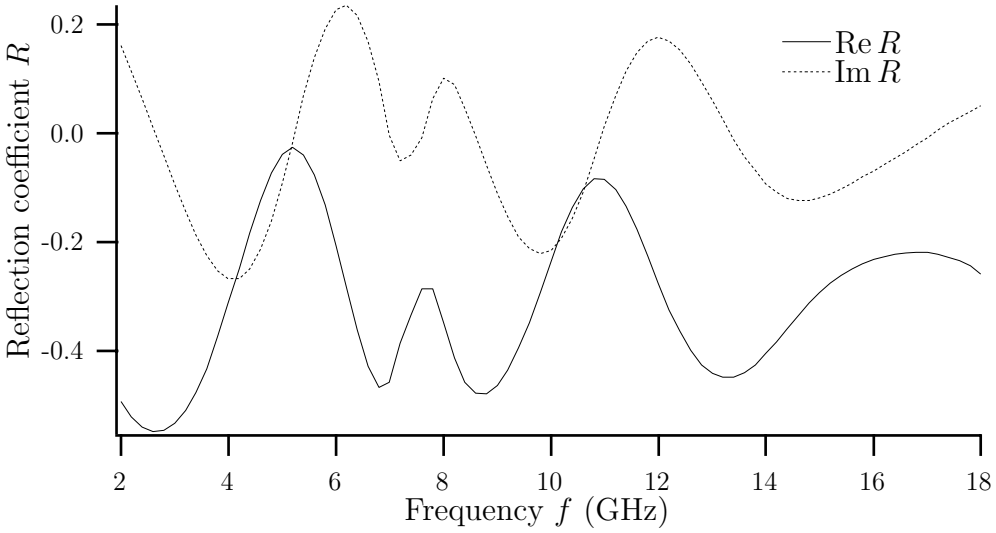

Figure 1: The synthetic reflection coefficient $R(\omega)$ at normal incidence for an isotropic chiral slab in the frequency-band 2–18 GHz. $\omega = 2\pi f$.

In compact matrix form — recall that the incident and scattered fields are two-dimensional — and with the space- and time-dependence suppressed, the solution to the scattering problem is [21]

$$\begin{pmatrix} \boldsymbol{E}^t \\ \boldsymbol{E}^r \end{pmatrix} = \begin{pmatrix} \mathbf{0} & \mathcal{R}_\infty \mathbf{I} \\ \mathcal{R}_\infty \mathbf{I} & \mathbf{0} \end{pmatrix} \cdot \begin{pmatrix} \boldsymbol{E}^i_{\text{left}} \\ \boldsymbol{E}^i_{\text{right}} \end{pmatrix} + (1 - \mathcal{R}_\infty^2) \left(1 - \mathcal{R}_\infty^2 \delta_{2\frac{d}{c}} * \mathcal{P}^2\right)^{-1} \\ \begin{pmatrix} \delta_{\frac{d}{c}} * \mathcal{P}^+ & -\mathcal{R}_\infty \delta_{2\frac{d}{c}} * \mathcal{P}^+ \cdot \mathcal{P}^- \\ -\mathcal{R}_\infty \delta_{2\frac{d}{c}} * \mathcal{P}^+ \cdot \mathcal{P}^- & \delta_{\frac{d}{c}} * \mathcal{P}^- \end{pmatrix} \cdot \begin{pmatrix} \boldsymbol{E}^i_{\text{left}} \\ \boldsymbol{E}^i_{\text{right}} \end{pmatrix},$$

where

$$\mathcal{R}_\infty = \left(\eta(1 + Z*) + \eta_0\right)^{-1} \left(\eta(1 + Z*) - \eta_0\right)$$

is the reflection operator for the corresponding semi-infinite medium,

$$\mathcal{P}^\pm = \exp\Big(\frac{d}{c}\frac{d}{dt}\big(-\mathbf{I}N \mp \mathbf{J}\chi_c\big) * \Big)\mathbf{I}$$

are the wave propagators of the slab for right-going and left-going waves, respectively, $\delta_a := \delta(t - a)$ is the time-delayed Dirac measure, and the asterisk is used to denote both convolution and dyadic dot product.

The propagators $\mathcal{P}^\pm$ are dyadic integral operators (with respect to time) interpreted as series expansions of the exponentials [21]. Observe that the wave propagators can be factored as

$$\mathcal{P}^\pm = \begin{cases} \mathcal{P}\mathcal{P}_c, \\ \mathcal{P}\mathcal{P}_c^{-1}, \end{cases}$$

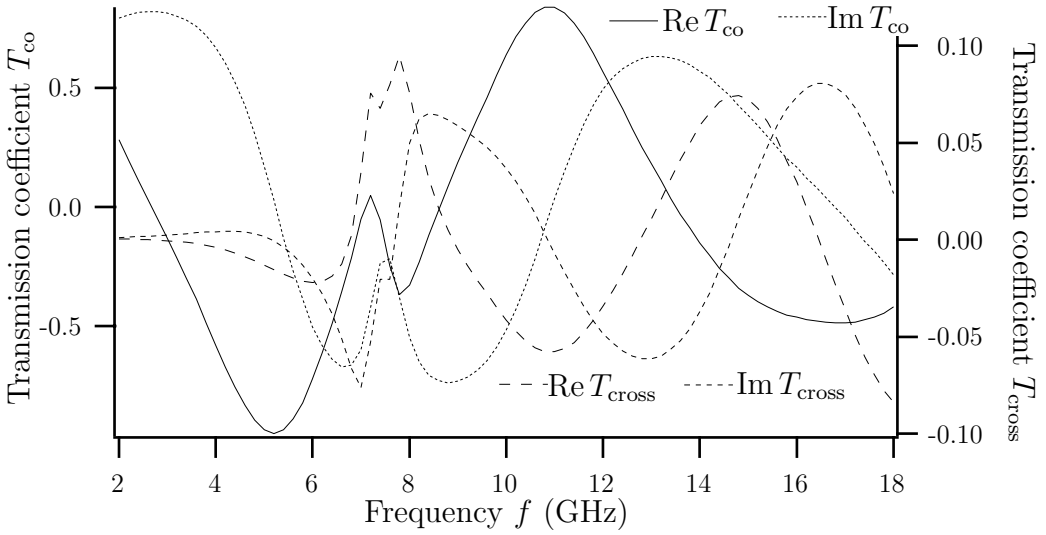

Figure 2: The synthetic transmission coefficients $T_{\rm co}(\omega)$ and $T_{\rm cross}(\omega)$ at normal incidence for an isotropic chiral slab in the frequency-band 2–18 GHz.

where the scalar (isotropic) propagator $\mathcal{P}$ is

$$\mathcal{P} = \exp\Big(-\frac{d}{c}\frac{d}{dt} N * \Big)$$

and where the propagator of revolution

$$\mathcal{P}_c = \exp\Big(-\frac{d}{c}\frac{d}{dt}\mathbf{J}\chi_c * \Big)\mathbf{I} = \mathbf{I}\cos\Big(-\frac{d}{c}\frac{d}{dt}\chi_c * \Big) + \mathbf{J}\sin\Big(-\frac{d}{c}\frac{d}{dt}\chi_c * \Big).$$

Note also the identity

$$\mathcal{P}^+ \cdot \mathcal{P}^- = \mathbf{I}\mathcal{P}^2,$$

which explains the absence of cross-reflection at normal incidence.

Recalling the geometric series shows that the integral operator

$$\Big(1 - \mathcal{R}_\infty^2 \delta_{2\frac{d}{c}} * \mathcal{P}^2\Big)^{-1}$$

present in the scattering relation represents multiple propagation through the slab. Similarly, the operator

$$1 - \mathcal{R}_\infty^2 = (1 - \mathcal{R}_\infty)(1 + \mathcal{R}_\infty)$$

is interpreted as a product of transmission operators. Mathematically, the above scattering relation has been obtained by using the wave-splitting concept. For further details on this time-domain problem, the reader is referred to [21].

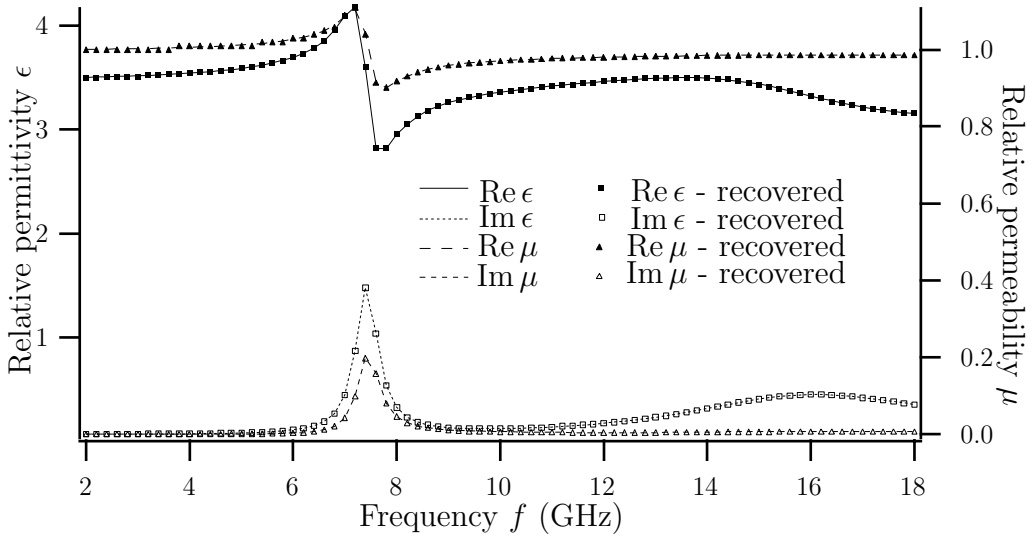

Figure 3: The permittivity $\epsilon(\omega)$ and permeability $\mu(\omega)$ for the isotropic chiral slab as a function of frequency f. These functions have been calculated from synthetic scattering data at normal incidence given in Figures 1 and 2. The medium is passive, since the imaginary parts of these properties are nonnegative.

2.2 Frequency-domain results

The spectral density of the electric field at the point $\boldsymbol{r}$ at the angular frequency ω is denoted by

$$\boldsymbol{E}(\boldsymbol{r},\omega) := \int_{-\infty}^{\infty} e^{i\omega t}\boldsymbol{E}(\boldsymbol{r},t)\,dt.$$

The spectral densities of other electromagnetic quantities are denoted analogously. As a consequence of this convention, the time dependence $e^{-i\omega t}$ at fixed frequency is understood.

The characterization

$$\begin{cases} \boldsymbol{D}(\boldsymbol{r},\omega) = \epsilon_0\epsilon(\omega)\boldsymbol{E}(\boldsymbol{r},\omega) + c_0^{-1}i\xi(\omega)\boldsymbol{H}(\boldsymbol{r},\omega), \\ \boldsymbol{B}(\boldsymbol{r},\omega) = -c_0^{-1}i\xi(\omega)\boldsymbol{E}(\boldsymbol{r},\omega) + \mu_0\mu(\omega)\boldsymbol{H}(\boldsymbol{r},\omega) \end{cases} \tag{2.1}$$

of the isotropic chiral medium is employed. These constitutive relations are used in [16] but with another time-convention ($e^{i\omega t}$). We say that the medium is dissipative (passive, lossy) at $\boldsymbol{r}$ if, cf. [16],

$$\text{Re}\,\{\nabla\cdot\boldsymbol{S}(\boldsymbol{r},\omega)\} \le 0 \text{ for all non-zero, non-static fields, } (\boldsymbol{E}(\boldsymbol{r},\omega),\boldsymbol{H}(\boldsymbol{r},\omega)), \tag{2.2}$$

where $\boldsymbol{S}(\boldsymbol{r},\omega) = \boldsymbol{E}(\boldsymbol{r},\omega)\times\boldsymbol{H}^*(\boldsymbol{r},\omega)/2$ is the complex Poynting vector at $\boldsymbol{r}$ at angular frequency ω. Furthermore, we say that the medium is active at $\boldsymbol{r}$ if

$$\text{Re}\,\{\nabla\cdot\boldsymbol{S}(\boldsymbol{r},\omega)\} > 0 \text{ for some non-zero, non-static fields, } (\boldsymbol{E}(\boldsymbol{r},\omega),\boldsymbol{H}(\boldsymbol{r},\omega)).$$

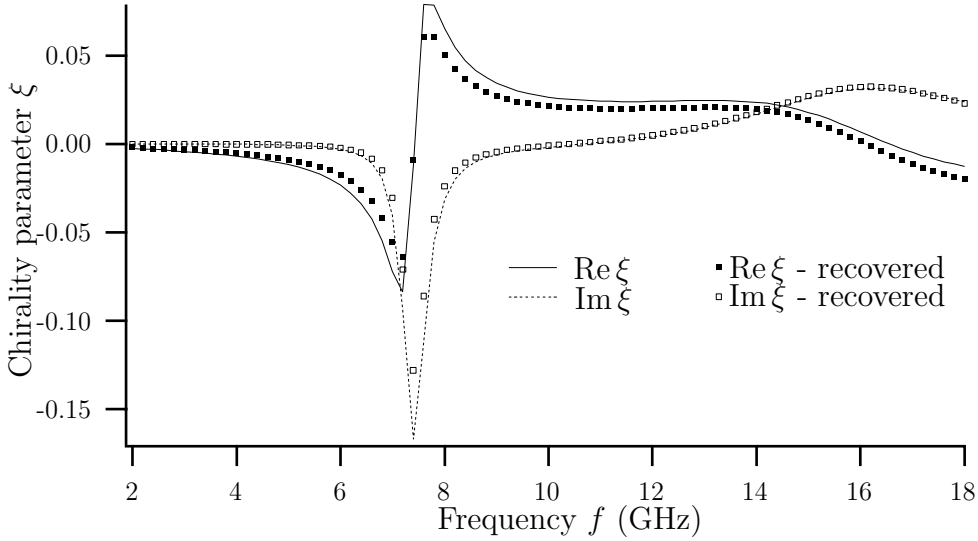

Figure 4: The chirality parameter $\xi(\omega)$ for an isotropic chiral slab as a function of frequency f. The chirality parameter depends solely on the synthetic transmission data presented in Figure 2.

Notice that this partition in terms of passive and active materials is exhaustive. We consider the lossless materials as a limit case of the passive materials: a medium is said to be lossless at $\boldsymbol{r}$ if

$$\text{Re}\,\{\nabla \cdot \boldsymbol{S}(\boldsymbol{r},\omega)\} = 0 \text{ for all non-zero, non-static fields, } (\boldsymbol{E}(\boldsymbol{r},\omega), \boldsymbol{H}(\boldsymbol{r},\omega)).$$

One can show that the homogeneous medium given by the constitutive relations (2.1) is passive if and only if [16]

$$\begin{cases} \text{Im}\,\epsilon(\omega) \geq 0, \\ \text{Im}\,\mu(\omega) \geq 0, \\ |\text{Im}\,\xi(\omega)| \leq \sqrt{\text{Im}\,\epsilon(\omega)\,\text{Im}\,\mu(\omega)} \end{cases} \tag{2.3}$$

for all $\omega \neq 0$. Moreover, the medium is lossless if the relative permittivity $\epsilon(\omega)$, the relative permeability $\mu(\omega)$, and the chirality parameter $\xi(\omega)$ all are real for all $\omega \neq 0$. The relation between these parameters and the time-domain constitutive parameters is readily obtained by Fourier transformation:

$$\begin{cases} \epsilon(\omega) = \epsilon_r^{\text{opt}}\big(1 + \chi_e(\omega)\big) = \epsilon_r^{\text{opt}}\dfrac{1 + N(\omega)}{1 + Z(\omega)}, \\ \mu(\omega) = \mu_r^{\text{opt}}\big(1 + \chi_m(\omega)\big) = \mu_r^{\text{opt}}\big(1 + N(\omega)\big)\big(1 + Z(\omega)\big), \\ \xi(\omega) = -i\chi_c(\omega)n^{\text{opt}}. \end{cases} \tag{2.4}$$

In the light of the results of Section 2.1, the time-harmonic constitutive relations

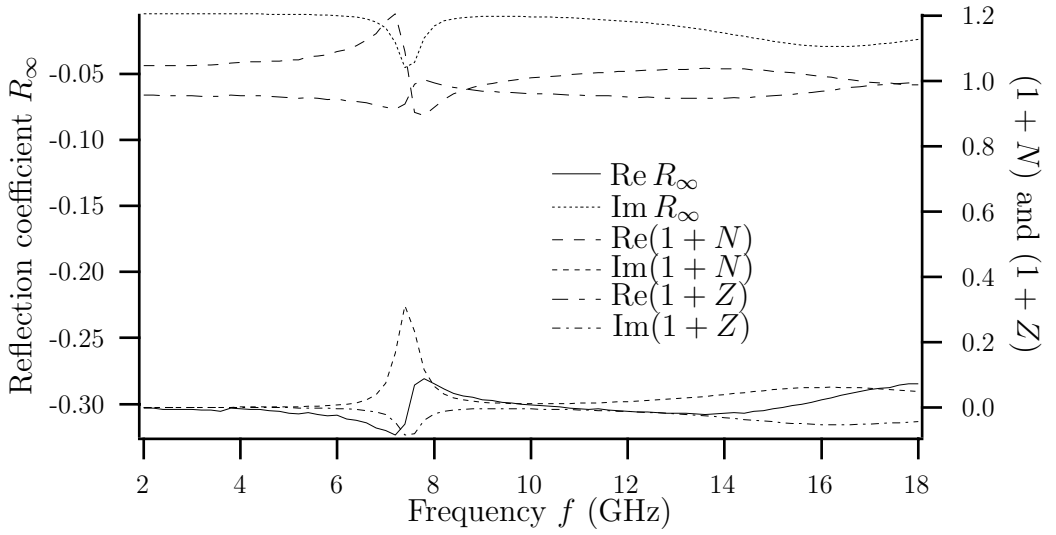

Figure 5: The properties $R_\infty(\omega)$, $1+N(\omega)$, and $1+Z(\omega)$ in the synthetic case as functions of frequency f.

can be written in the form

$$\begin{cases} \eta\big(1+Z(\omega)\big)\boldsymbol{D}(\boldsymbol{r},\omega) = c^{-1}\big(1+N(\omega)\big)\boldsymbol{E}(\boldsymbol{r},\omega) + c^{-1}\chi_c(\omega)\eta\big(1+Z(\omega)\big)\boldsymbol{H}(\boldsymbol{r},\omega), \\ \boldsymbol{B}(\boldsymbol{r},\omega) = -c^{-1}\chi_c(\omega)\boldsymbol{E}(\boldsymbol{r},\omega) + c^{-1}\big(1+N(\omega)\big)\eta\big(1+Z(\omega)\big)\boldsymbol{H}(\boldsymbol{r},\omega). \end{cases}$$

Similarly, the scattering relation at normal incidence for the bi-isotropic slab $(0,d)$ reads

$$\begin{pmatrix} \boldsymbol{E}^t(\omega) \\ \boldsymbol{E}^r(\omega) \end{pmatrix} = \begin{pmatrix} \mathbf{0} & R_\infty(\omega)\mathbf{I} \\ R_\infty(\omega)\mathbf{I} & \mathbf{0} \end{pmatrix} \cdot \begin{pmatrix} \boldsymbol{E}^i_{\text{left}}(\omega) \\ \boldsymbol{E}^i_{\text{right}}(\omega) \end{pmatrix} + \frac{1-R^2_\infty(\omega)}{1-R^2_\infty(\omega)P^2(\omega)} \\ \begin{pmatrix} \mathbf{P}^+(\omega) & -R_\infty(\omega)\mathbf{P}^+(\omega)\cdot\mathbf{P}^-(\omega) \\ -R_\infty(\omega)\mathbf{P}^+(\omega)\cdot\mathbf{P}^-(\omega) & \mathbf{P}^-(\omega) \end{pmatrix} \cdot \begin{pmatrix} \boldsymbol{E}^i_{\text{left}}(\omega) \\ \boldsymbol{E}^i_{\text{right}}(\omega) \end{pmatrix},$$

where

$$R_\infty(\omega) = \frac{\eta\big(1+Z(\omega)\big)-\eta_0}{\eta\big(1+Z(\omega)\big)+\eta_0} \tag{2.5}$$

is the reflection coefficient of the corresponding half-space, whereas

$$\mathbf{P}^\pm(\omega) = \exp\left(i\omega\frac{d}{c}\big(\mathbf{I}(1+N(\omega)) \pm \mathbf{J}\chi_c(\omega)\big)\cdot\right)\mathbf{I} = \begin{cases} P(\omega)\mathbf{P}_c(\omega), \\ P(\omega)\mathbf{P}_c^{-1}(\omega), \end{cases} \tag{2.6}$$

$$P(\omega) = \exp\left(i\omega\frac{d}{c}\big(1+N(\omega)\big)\right), \tag{2.7}$$

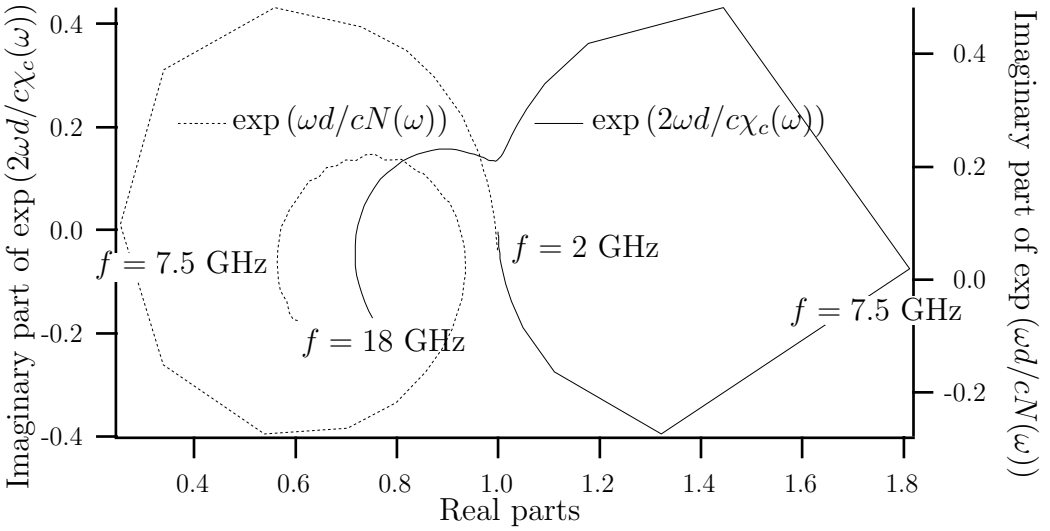

Figure 6: The behavior of the exponentials $\exp\left(2\omega\frac{d}{c}\chi_c(\omega)\right)$ and $\exp\left(i\omega\frac{d}{c}N(\omega)\right)$ in the complex plane in the synthetic case. Since neither of these curves embraces the origin, the principal branch of the logarithm generates correct values of $\chi_c(\omega)$ and $N(\omega)$.

and

$$\mathbf{P}_c(\omega) = e^{i\omega\frac{d}{c}\chi_c(\omega)\mathbf{J}}\cdot\mathbf{I} = \mathbf{I}\cos\left(i\omega\frac{d}{c}\chi_c(\omega)\right) + \mathbf{J}\sin\left(i\omega\frac{d}{c}\chi_c(\omega)\right) \tag{2.8}$$

are the propagation factors of the slab. These are the analogues to the wave propagators defined in Section 2.1. Note that the time-delay d/c has been included in the propagation factors $\mathbf{P}^{\pm}(\omega)$ and $P(\omega)$.

From equation (2.8), it follows that the real part of $\xi(\omega) = -i\chi_c(\omega)n^{\text{opt}}$ is the origin of ORP (optical rotatory power), whereas the imaginary part causes the CD distortion (circular dichroism). Thus, the transmitted wave is generally elliptically polarized.

The results presented in this Section are in agreement with equations (69)–(71) in the investigation by Bassiri *et al.* [1], obtained by considering the right- and left-hand circularly polarized eigenwaves. The propagation factors of the circularly polarized waves

$$P_{\pm}(\omega) = \exp\left(i\omega\frac{d}{c}\big(1 + N(\omega) \pm i\chi_c(\omega)\big)\right)$$

arise when Euler's formulae are applied to equation (2.8):

$$\mathbf{P}^{\pm}(\omega) = P_{\pm}(\omega)\frac{(\mathbf{I} - i\mathbf{J})}{2} + P_{\mp}(\omega)\frac{(\mathbf{I} + i\mathbf{J})}{2}.$$

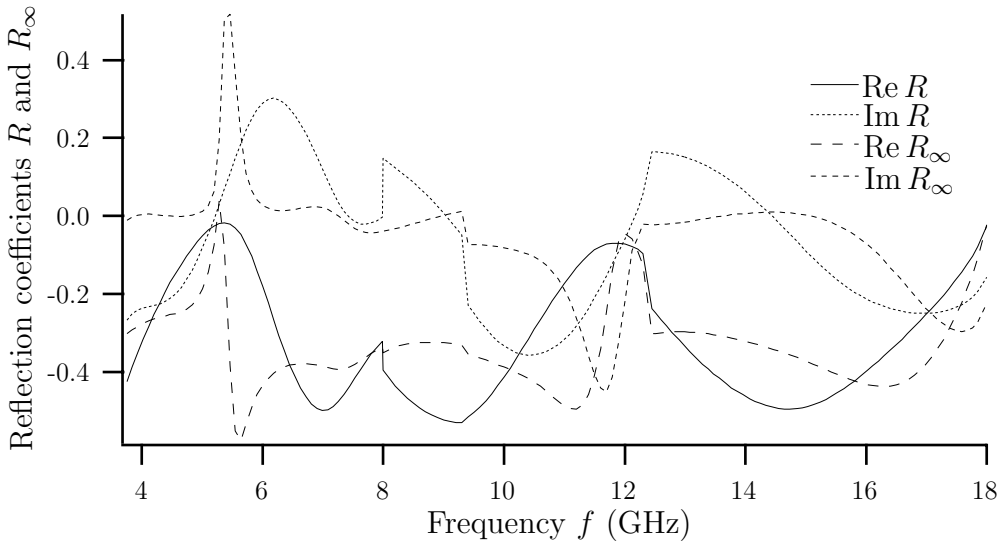

Figure 7: The reflection coefficient $R(\omega)$ at normal incidence for a man-made isotropic chiral slab in the frequency band 3.5–18 GHz. The Weir parameter (the reflection coefficient for the half-space) $R_\infty(\omega)$ is presented also.

3 Inverse scattering in the frequency domain

In this section, the inverse scattering problem in the frequency domain is analyzed. This problem is to compute the constitutive parameters $\epsilon(\omega)$, $\mu(\omega)$, and $\xi(\omega)$ from scattering data. The scattering relation obtained in the previous section shows that two-sided excitation of the isotropic chiral slab is superfluous.

If $\boldsymbol{E}^i_{\text{right}}(\omega) := \mathbf{0}$ and $\boldsymbol{E}^i(\omega) := \boldsymbol{E}^i_{\text{left}}(\omega)$, the scattering relation reads

$$\begin{cases} \boldsymbol{E}^r(\omega) = R(\omega)\boldsymbol{E}^i(\omega), \\ \boldsymbol{E}^t(\omega) = \mathbf{T}(\omega) \cdot \boldsymbol{E}^i(\omega). \end{cases} \tag{3.1}$$

The reflection coefficient $R(\omega)$ and the transmission dyadic $\mathbf{T}(\omega)$ are easily computed from time-harmonic scattering data, $\boldsymbol{E}^r(\omega)$ and $\boldsymbol{E}^t(\omega)$, and the known excitation $\boldsymbol{E}^i(\omega)$. Due to axial symmetry of the medium, one has

$$\mathbf{T}(\omega) \equiv \mathbf{I}T_{\text{co}}(\omega) + \mathbf{J}T_{\text{cross}}(\omega).$$

Comparison with results in the previous section yields the explicit expressions

$$\begin{cases} R(\omega) = \left(1 - \dfrac{\big(1 - R^2_\infty(\omega)\big)P^2(\omega)}{1 - R^2_\infty(\omega)P^2(\omega)}\right) R_\infty(\omega), \\ \mathbf{T}(\omega) = \dfrac{\big(1 - R^2_\infty(\omega)\big)P(\omega)}{1 - R^2_\infty(\omega)P^2(\omega)}\mathbf{P}_c(\omega) \end{cases} \tag{3.2}$$

for the reflection coefficient and the transmission matrix.

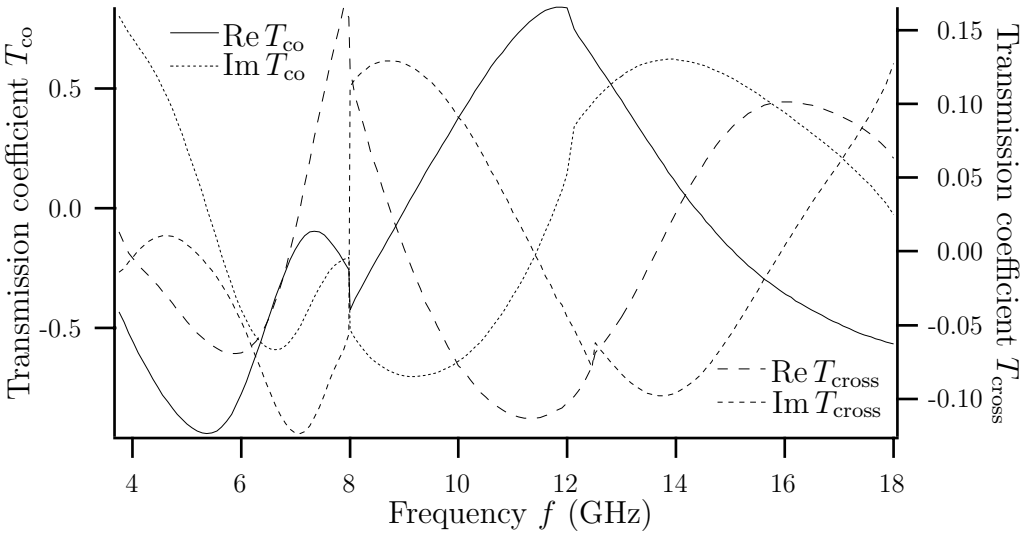

Figure 8: The transmission coefficients $T_{\rm co}(\omega)$ and $T_{\rm co}(\omega)$ at normal incidence for a man-made isotropic chiral slab in the frequency band 3.5–18 GHz.

The first step in the proposed inverse algorithm is to compute the chiral parameter $\chi_c(\omega)$. To this end, define a scalar transmission coefficient as

$$\mathbf{I}T(\omega) := \mathbf{P}_c^{-1}(\omega) \cdot \mathbf{T}(\omega).$$

This is equivalent to

$$\begin{cases} T(\omega) = T_{\rm co}(\omega)\, \cos\left(-i\omega\dfrac{d}{c}\chi_c(\omega)\right) - T_{\rm cross}(\omega)\, \sin\left(-i\omega\dfrac{d}{c}\chi_c(\omega)\right), \\ 0 = T_{\rm co}(\omega)\, \sin\left(-i\omega\dfrac{d}{c}\chi_c(\omega)\right) + T_{\rm cross}(\omega)\, \cos\left(-i\omega\dfrac{d}{c}\chi_c(\omega)\right). \end{cases} \tag{3.3}$$

The second of these identities determines $\chi_c(\omega)$, and once this property is known, $T(\omega)$ is obtained by the first. Consequently, the scattering relation (3.2) reduces to

$$\begin{cases} R(\omega) = \big(1 - P(\omega)T(\omega)\big)R_\infty(\omega), \\ T(\omega) = \dfrac{\big(1 - R_\infty^2(\omega)\big)P(\omega)}{1 - R_\infty^2(\omega)P^2(\omega)}. \end{cases} \tag{3.4}$$

In the achiral case, $T_{\rm cross}(\omega) = 0$ and $T(\omega) = T_{\rm co}(\omega)$ is precisely the transmission coefficient. Applying Euler's formulae to the second identity (3.3) yields the transcendental equation

$$e^{2\omega\frac{d}{c}\chi_c(\omega)} = T_{\rm quotient}(\omega), \tag{3.5}$$

where the right hand side is

$$T_{\rm quotient}(\omega) = \frac{T_{\rm co}(\omega) - iT_{\rm cross}(\omega)}{T_{\rm co}(\omega) + iT_{\rm cross}(\omega)} = Q\left(\frac{iT_{\rm cross}(\omega)}{T_{\rm co}(\omega)}\right)$$

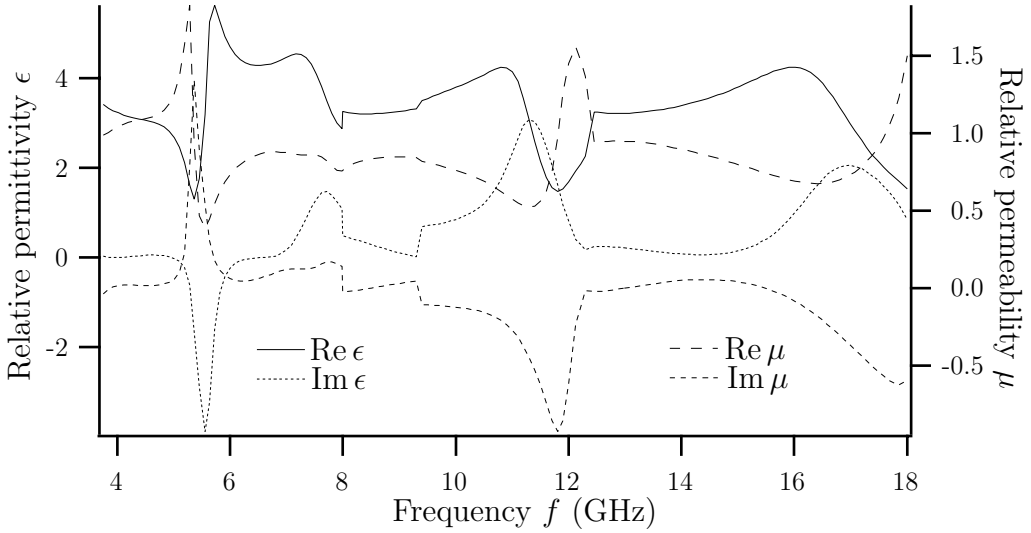

Figure 9: The relative permittivity $\epsilon(\omega)$ and permeability $\mu(\omega)$ for a man-made isotropic chiral slab as a function of frequency f. These functions have been calculated from scattering data at normal incidence given in Figures 7 and 8. For a passive medium, the imaginary parts of these properties are nonnegative.

and $Q(x) = (1-x)/(1+x)$ is the frequently encountered quotient function [15]. For a small chirality parameter, $T_{\text{quotient}}(\omega) \approx 1$. A solution to this equation is

$$2\omega\frac{d}{c}\chi_c(\omega) = \text{Superlog}\big(T_{\text{quotient}}(\omega)\big),$$

where the function Superlog coincides with the principle branch of the logarithm at low frequencies, and, furthermore, in order to preserve the continuity of $\chi_c(\omega)$, is designed to add $\pm 2\pi i$ to the result when the curve $T_{\text{quotient}}(\omega)$ cuts the negative real axis. It should be observed that the proposed method may fail if the sampling in frequency is not dense enough or if low-frequency data is not available. The result can be checked in the high-frequency limit by the Riemann-Lebesgue lemma: $\chi_c(\omega)$ approaches 0 as ω tends to infinity.

In the second step, $P(\omega)$ and $R_\infty(\omega)$ are determined from $T(\omega)$ and $R(\omega)$. Another way to state the scattering relation (3.4) is

$$\begin{cases} R(\omega) = \big(1 - P(\omega)T(\omega)\big)R_\infty(\omega), \\ T(\omega) = \big(1 - R_\infty(\omega)R(\omega)\big)P(\omega). \end{cases}$$

Eliminating $P(\omega)$ in the first equation and $R_\infty(\omega)$ in the second equation yield the polynomial equations of the second degree

$$\begin{cases} R_\infty^2(\omega)R(\omega) - R_\infty(\omega)\left(1 + R^2(\omega) - T^2(\omega)\right) + R(\omega) = 0, \\ P^2(\omega)T(\omega) - P(\omega)\left(1 + T^2(\omega) - R^2(\omega)\right) + T(\omega) = 0, \end{cases}$$

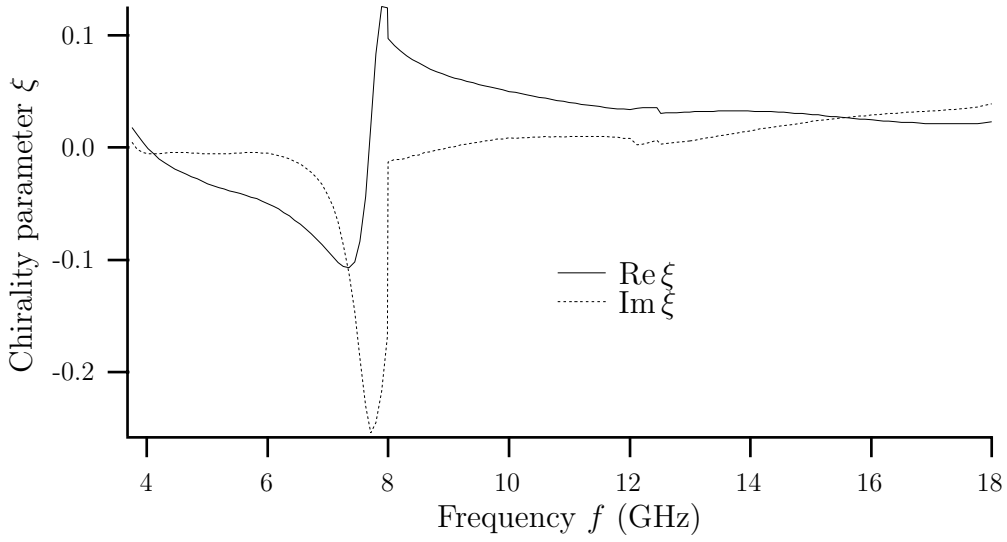

Figure 10: The chirality parameter $\xi(\omega)$ for a man-made isotropic chiral slab as a function of frequency f. The chirality parameter depends solely on the transmission data presented in Figure 8.

which have the solutions

$$\begin{cases} R_\infty(\omega) = \dfrac{1 + R^2(\omega) - T^2(\omega) - \sqrt{(1 + R^2(\omega) - T^2(\omega))^2 - 4R^2(\omega)}}{2R(\omega)}, \\ P(\omega) = \dfrac{1 + T^2(\omega) - R^2(\omega) - \sqrt{(1 + T^2(\omega) - R^2(\omega))^2 - 4T^2(\omega)}}{2T(\omega)}. \end{cases}$$

In particular, for the nonreflective ($R(\omega)$=0) isotropic chiral medium, one obtains $P(\omega) = T(\omega)$, which is the correct root. For the semi-infinite medium, $T(\omega) \equiv 0$, and one obtains $R_\infty(\omega) = R(\omega)$, which also is the correct root. Note also that since

$$\mathbf{I}T^2(\omega) = \mathbf{T}(\omega) \cdot \mathbf{T}(\omega)^t = \mathbf{I}\left(T_{\text{co}}^2(\omega) + T_{\text{cross}}^2(\omega)\right),$$

$R_\infty(\omega)$ is independent of $\chi_c(\omega)$ and depends on scattering data only. Once $R_\infty(\omega)$ is known, the dispersive factor $1 + Z(\omega)$ of the intrinsic impedance is obtained from (2.5):

$$1 + Z(\omega) = \frac{1}{\eta_r^{\text{opt}}} \frac{1 + R_\infty(\omega)}{1 - R_\infty(\omega)}.$$

In the third step, the property $N(\omega)$ is recovered from equation (2.7):

$$e^{i\omega\frac{d}{c}N(\omega)} = P(\omega)e^{-i\omega\frac{d}{c}}.$$

The technique of reconstruction is similar to the one used to obtain the chirality parameter $K(\omega)$; it is assumed that the solution is given by

$$i\omega\frac{d}{c}N(\omega) = \text{Superlog}\big(P(\omega)e^{-i\omega\frac{d}{c}}\big).$$

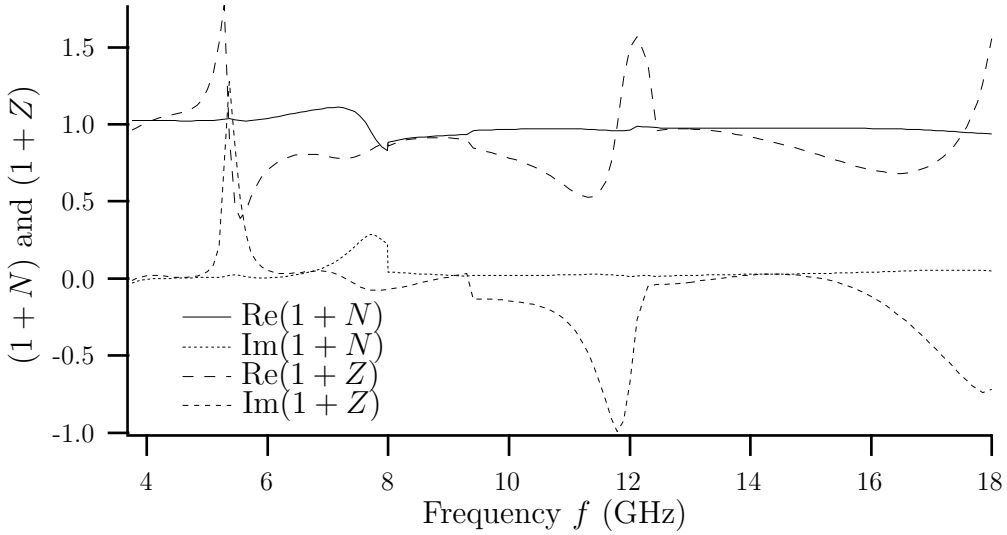

Figure 11: The properties $1+N(\omega)$ and $1+Z(\omega)$ for a man-made isotropic chiral slab as functions of frequency f.

By the Riemann-Lebesgue lemma, $N(\omega)$ approaches 0 as ω tends to infinity.

In the fourth and final step, the relative permittivity $\epsilon(\omega)$, the relative permeability $\mu(\omega)$, and the chirality parameter $\xi(\omega)$ are obtained from equation (2.4) by straightforward multiplication. By inverse Fourier transformation, the time-dependent susceptibility functions can be obtained as well.

4 Numerical results

Codes implemented in the MATLAB environment have been developed both for the direct scattering problem and the inverse scattering problem. In this section the inversion algorithm presented above is tested numerically.

The constitutive parameters of a realistic multiple-resonance isotropic chiral medium as functions of frequency are given in Figures 3 and 4. Furthermore, $\epsilon_r^{\rm opt} = 3.2$ and $\mu_r^{\rm opt} = 1$. The MTWC-code has been used to generate the synthetic scattering data at normal incidence [18, 19]. Reflection and transmission data are presented in Figures 1 and 2. The results of the inversion are also shown in Figures 3 and 4 represented by markers. Since the chirality parameter $\xi(\omega)$ is small, it is not surprising that the relative error is larger in the reconstruction of this property than in the recovery of the permittivity $\epsilon(\omega)$ and the permeability $\mu(\omega)$. The properties $R_\infty(\omega)$, $1+N(\omega)$, and $1+Z(\omega)$ as functions of frequency are found in Figure 5. The traces of the exponentials $\exp\left(2\omega\frac{d}{c}\chi_c(\omega)\right)$ and $\exp\left(i\omega\frac{d}{c}N(\omega)\right)$ in the complex plane are shown in Figure 6. Note that these curves do not enter the left half-plane; therefore, the principal branch of the logarithm generates the correct values of $\chi_c(\omega)$ and $N(\omega)$ throughout the frequency-band.

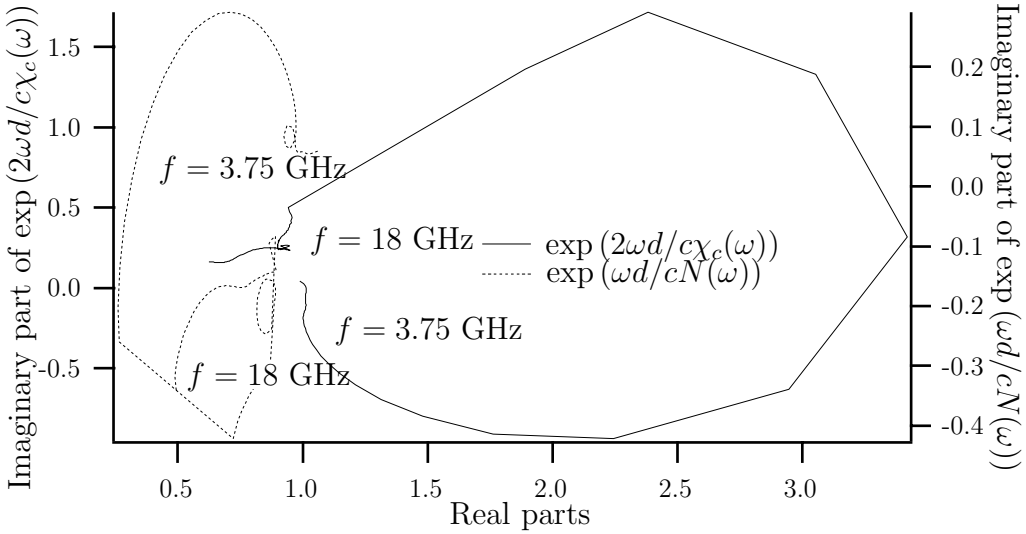

Figure 12: The behavior of the exponentials $\exp\left(2\omega\frac{d}{c}\chi_c(\omega)\right)$ and $\exp\left(i\omega\frac{d}{c}N(\omega)\right)$ in the complex plane in the experimental case. The principal branch of the logarithm generates correct values of $\chi_c(\omega)$ and $N(\omega)$.

5 Inversion based on experimental measurements

In this section we present scattering data at normal incidence from a specific man-made chiral slab. Data and results of inversion are presented in Figures 7–12. The experimental setup is depicted in Figure 14.

Free-space measurements are made using a vectorial network analyzer HP 8510C from 3.5 to 18 GHz. Elliptic reflectors are used to focus the beam on the slab, in order to obtain a plane wave at the position of the object and to reduce the interference effects between the measurement and the surrounding environment. To cover this wide frequency range, we are using two kind of elliptic reflectors (one for 3.5 to 8 GHz and one from 8 to 18 GHz). The electromagnetic field is generated using three different horn antennas (3.5–8 GHz, 8–12 GHz and 12–18 GHz). The horns are located at the first focus of the elliptic reflectors while the sample is located at the second one. In order to bypass the use of an anechoic protection, measurements are performed using the time-domain option of the analyzer. After a calibration of the device, measurements are first made in the frequency domain. The internal Fourier-transform features of the analyzer allows one to obtain the time-domain response. This signal is filtered in order to eliminate the multiple reflections due to the environment. Then, an inverse Fourier transform gives the response of the object in the frequency domain.

The sample is a square plate of size 300 × 300 mm, larger than the spot. The thickness of the slab is d=15 mm. Reflection and transmission coefficients measurements are performed. In a classic way, reference signals are obtained with a metallic plate and no sample at the measurement platform. We are also able to measure bistatic reflection, transmission and radiation patterns. The bench is driven by

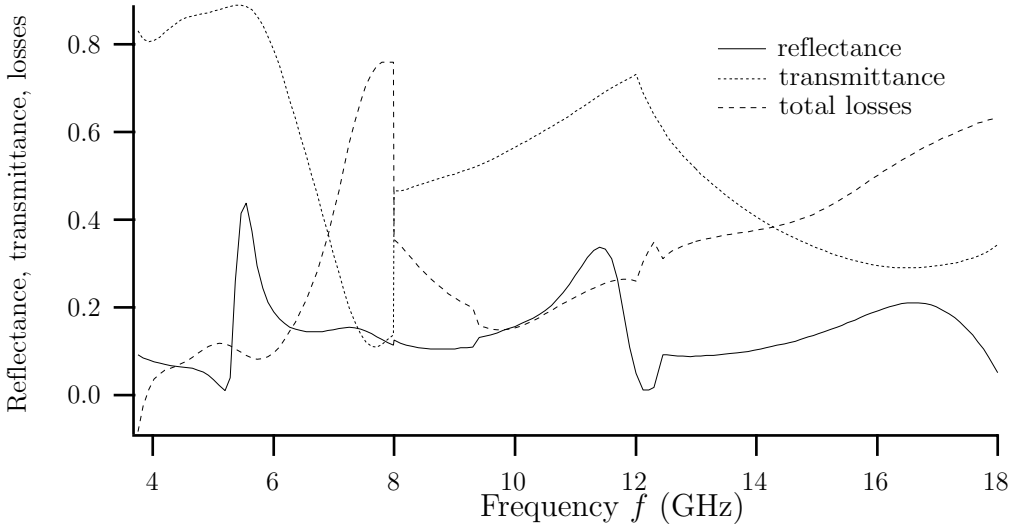

Figure 13: The reflectance $|R(\omega)|^2$, the transmittance $|T_{\rm co}(\omega)|^2 + |T_{\rm cross}(\omega)|^2$, and the loss function $1 - |R(\omega)|^2 - |T_{\rm co}(\omega)|^2 - |T_{\rm cross}(\omega)|^2$ at normal incidence for a man-made isotropic chiral slab in the frequency band 3.5–18 GHz.

two stepping motors that allow rotation of the receiving antennas and the sample support (see Figure 14).

The main drawback of this measurement procedure is due to the calibration method. Indeed, the reflection and transmission measurements are most accurate for the amplitude of the fields, but the simple calibration does not allow good precision on the phase measurements. The lack of precision must be related to the positioning of the sample or the antennas; the shift in this positioning induces a shift in the experimental phase. Consequently, the errors in the phase are greater with free space techniques than with guided waves methods. A solution could be to improve the calibration of the bench in order to decrease the phase measurement errors.

The sample consists of identical left-handed, one-turn helices uniformly and randomly embedded in an isotropic host medium, characterized by $\epsilon_r^{\rm opt} = 3.2$ and $\mu_r^{\rm opt} = 1$. The dimensions of the helices are: radius=1.65 mm, pitch=2.0 mm, wire gauge=0.3 mm. The number of helices per unit volume is 3.1. These data have been used to generate the synthetic data in Section 4.

Experimental scattering data is presented in Figures 7 and 8. In Figure 13, the reflectance $|R(\omega)|^2$ and the transmittance $|T_{\rm co}(\omega)|^2 + |T_{\rm cross}(\omega)|^2$ are shown, and the function $1 - |R(\omega)|^2 - |T_{\rm co}(\omega)|^2 - |T_{\rm cross}(\omega)|^2$ that represents the losses in the slab is presented also. The result of the inversion of scattering data is shown in Figures 9 and 10. Note that the chirality parameter is very similar to the one in the numerical example. Note also that several resonance peaks are present in the permittivity and the permeability. Furthermore, note that the imaginary parts of the permittivity and permeability are negative for high and for low frequencies, modeling a nondissipative (active) medium. The properties $1 + N(\omega)$ and $1 + Z(\omega)$ as functions of frequency are found in Figure 11 and the reflection coefficient for the corresponding half-space,

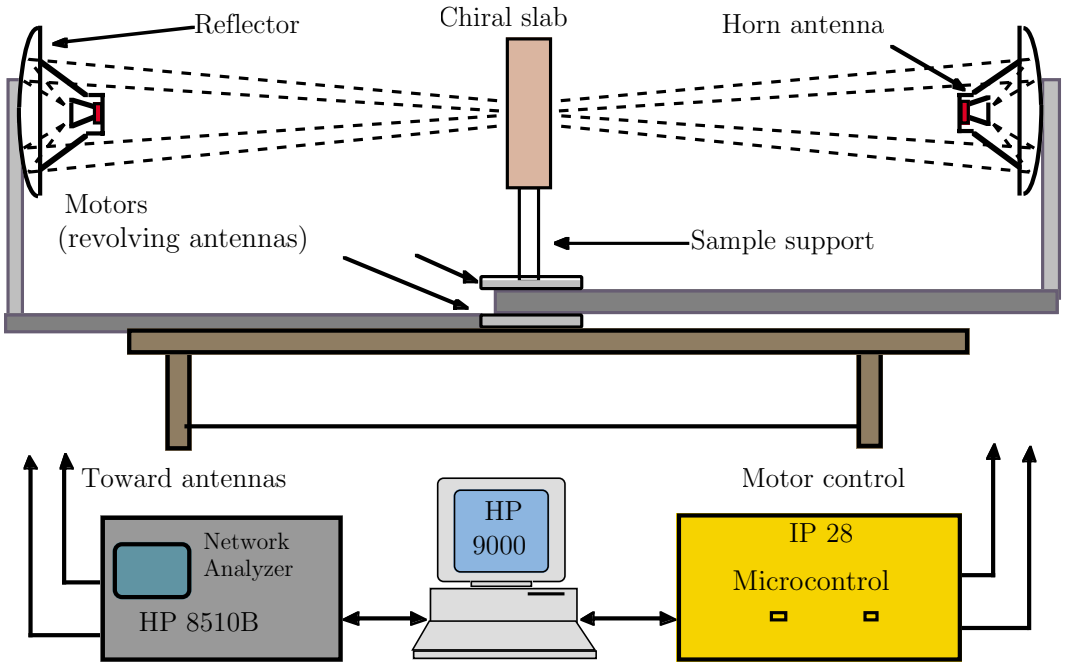

Figure 14: Experimental set-up

$R_\infty(\omega)$, is depicted in Figure 7. The trace of the exponentials $\exp\left(2\omega\frac{d}{c}\chi_c(\omega)\right)$ and $\exp\left(i\omega\frac{d}{c}N(\omega)\right)$ in the complex plane are shown in Figure 12.

6 Discussion

We have developed independent codes both for the direct scattering problem and the inverse scattering problem. Applying the inverse code on synthetic scattering data reproduces the material parameters; therefore, we expect the numerical codes to be correct. Applying the inverse code on experimental data in the range 3.5–18 GHz shows that several resonance phenomena occur in the chiral medium. Some of these are possible to foresee on theoretical grounds: the synthetic scattering data presented in this paper is a result of such an attempt.

In particular, we notice that the passivity condition (2.3) is violated. This condition was also violated in [25, 26]. However, Figure 13 indicates that, basically, scattering data are sound.

Several explanations for this are possible. One is that it is difficult to obtain reliable scattering data in these bands as explained in Section 5. Another explanation is that there are physical (thermodynamical) mechanisms involved that we have not considered or that the underlying model (2.1) is not complete and has to be modified. The assumption that the chiral composite material is homogeneous is also debatable as was pointed out in [26].

On the basis of the results presented in this paper and in [25, 26], the passivity condition (2.3) seems to be too austere. Figure 13 shows that the chiral material

generates presumably sound scattering data at normal incidence although it is not passive according to definition (2.2). On the other hand there may be other excitations — pathological or nonpathological — that generate "unsound" scattering data. This is not a contradiction but merely reflects the definition of passivity (2.2).

Finally, we notice that the index of refraction, which is the relevant material property at wave propagation, principally look sound (compare the results for synthetic and experimental data). This is in concordance with a sentence in [3]. Plotting the refractive indices of the RCP and LCP eigenwaves shows that these quantities principally look sound also. For instance, their imaginary parts are positive giving rise to solutions that are exponentially decaying in the direction of propagation. However, the fact that the solutions are exponentially decaying is not connected to passivity in the sense of definition (2.2).

7 Conclusion

We have been developed an alternative rigorous method for obtaining the constitutive parameters of an isotropic chiral medium from scattering data at normal incidence. Furthermore, measurements on a man-made slab have been presented as well as reconstructions of the permittivity, the permeability, and the chirality parameters of the medium. On the basis of the results of reconstruction, the question whether the passivity concept (2.2) is useful has been raised. By restricting the function space in (2.2) strongly, it can be argued that the reconstructed permittivity and permeability, and chirality functions do not violate a condition corresponding to (2.2). We will discuss this matter in a more general case in a forthcoming article.

8 Acknowledgment

The work reported in this paper is supported by a grant from the Swedish Research Council for Engineering Sciences, and its support is gratefully acknowledged. A research grant from CEA/CESTA is also gratefully acknowledged ("Etude analyticque de l'interaction d'une impulsion courte avec un matriau dispersif").

References

[1] S. Bassiri, C. H. Papas, and N. Engheta. Electromagnetic wave propagation through a dielectric-chiral interface and through a chiral slab. *J. Opt. Soc. Am.*, **A5**, 9, 1988.

[2] S. Breton, Ph. Talbot, Ph. Gelin, and F. Mariotte. Etude electromagnetique d'une cellule de caracterisation en bande X de materiaux chiraux. In *JCMM94 Proceedings*, Brest, France, October 1994.

[3] G. Busse and A. F. Jacob. Measurement techniques for characterizing handed microwave media. In Werner S. Weiglhofer, editor, *Proceedings of Bianisotrop-*

ics'97, pages 31–38, University of Glasgow, Great Britain, 1997. Department of Mathematics.

[4] G. Busse, J. Reinert, M. Klemt, and A. F. Jacob. On chirality measurements in circular waveguides. In A. Priou, A. Sihvola, S. Tretyakov, and A. Vinogradov, editors, *Advances in complex electromagnetic materials*, pages 333–340, Dordrecht/Boston/London, 1996. Kluwer Academic Publishers Group. Proceedings of the Advanced Research Workshop on Electromagnetics of Chiral, Bi-isotropic, and Bi-anisotropic Media (Chiral'96), St. Petersburg—Moscow, 23–30 July 1996.

[5] J. H. Cloete and A. G. Smith. The constitutive parameters of a lossy chiral slab by inversion of plane-wave scattering coefficients. *Microwave Opt. Techn. Lett.*, **5**, 303–306, 1992. Correction: Vol., No.1, 1994.

[6] Johannes Hendrik Cloete. The status of experimental research on chiral composites. In Werner S. Weiglhofer, editor, *Proceedings of Bianisotropics'97*, pages 39–42, University of Glasgow, Great Britain, 1997. Department of Mathematics.

[7] N. Engheta and D. L. Jaggard. Electromagnetic chirality and its applications. *IEEE Antennas and Propagation Society Newsletter*, pages 6–12, October 1988.

[8] F. Guérin, V. K. Varadan, V. V. Varadan, M. Labeyrie, and P. Y. Guillon. Some experimental results on the dispersive behaviour of chiral composites. *J. Phys. D: Applied Phys.*, **28**, 194–201, 1995.

[9] A. Karlsson and G. Kristensson. Constitutive relations, dissipation and reciprocity for the Maxwell equations in the time domain. *J. Electro. Waves Applic.*, **6**(5/6), 537–551, 1992.

[10] G. Kristensson and S. Rikte. The inverse scattering problem for a homogeneous bi-isotropic slab using transient data. In L. Päivärinta and E. Somersalo, editors, *Inverse Problems in Mathematical Physics*, pages 112–125. Springer-Verlag, Berlin, 1993.

[11] G. Kristensson and S. Rikte. Transient wave propagation in reciprocal bi-isotropic media at oblique incidence. *J. Math. Phys.*, **34**(4), 1339–1359, 1993.

[12] G. Kristensson, S. Rikte, and A. Sihvola. Mixing formulas in the time domain. *J. Opt. Soc. Am. A*, 1998. Accepted for publication.

[13] A. Lakhtakia. Recent contributions to classical electromagnetic theory of chiral media: what next? *Speculations in Science and Technology*, **14**(1), 2–17, 1991.

[14] A. Lakhtakia, V. K. Varadan, and V. V. Varadan. *Time-Harmonic Electromagnetic Fields in Chiral Media*, volume 335 of *Lecture Notes in Physics*. Springer-Verlag, New York, 1989.

[15] I. V. Lindell and A. H. Sihvola. The quotient function and its applications. *Am. J. Phys*, **66**(3), 197–202, 1998.

[16] I. V. Lindell, A. H. Sihvola, S. A. Tretyakov, and A. J. Viitanen. *Electromagnetic Waves in Chiral and Bi-isotropic Media*. Artech House, Boston, London, 1994.

[17] Raymond Luebbers, H. Scott Langdon, Forrest Hunsberger, Craig F. Bohren, and Shoko Yoshikawa. Calculation and measurement of the effective chirality parameter of a composite chiral material over a wide frequency band. *IEEE Trans. Antennas Propagat.*, **43**(2), 123–130, 1995.

[18] F. Mariotte, B. Sauviac, and J. Ph. Heliot. Heterogeneous chiral materials modelling (MTWC model): theory, comparison with experimental results and applications. *Journal of Physics III*, **5**(10), 1537–1564, October 1995.

[19] F. Mariotte, S.A. Tretyakov, and B. Sauviac. Modeling effective properties of chiral composites. *IEEE Antennas and Propagation Magazine*, **39**(2), 22–32, April 1996.

[20] S. Ougier. *Modelisation et Caracterisation de Materiaux Chiraux dans le Domaine des Microondes*. PhD thesis, Universite Paul Sabatier, Toulouse, France, 1993.

[21] S. Rikte. The Theory of the Propagation of TEM-Pulses in Dispersive Bi-isotropic Slabs. Technical Report LUTEDX/(TEAT-7040)/1–22/(1995), Lund Institute of Technology, Department of Electromagnetic Theory, P.O. Box 118, S-211 00 Lund, Sweden, 1995.

[22] S. Rikte. Reconstruction of bi-isotropic material parameters using transient electromagnetic fields. *Wave Motion*, **28**(1), July 1998. Scheduled for publication.

[23] L. H. Ruotanen and A. Hujanen. Simple derivation of constitutive parameters of isotropic chiral slab from wideband measurement data. *Microwave Opt. Techn. Lett.*, **12**(1), 40–45, 1996.

[24] L. H. Ruotanen and A. Hujanen. Experimental verification of physical conditions restricting chiral material parameters. *J. Electro. Waves Applic.*, **11**(1), 21–35, 1997.

[25] A. G. Smith, S. Kuehl, and J. H. Cloete. Experimental characterization of artificial chiral materials at microwave frequencies. In *IEEE/SAIEE AP/MTTS-93 Proceedings*, 1993.

[26] V. V. Varadan, R. Ro, and V. K. Varadan. Measurement of the electromagnetic properties of chiral composite materials in the 8–40 GHz range. *Radio Sci.*, **29**, 9–22, 1994.

[27] W. B. Weir. Automatic measurement of complex dielectric constant and permeability at microwave frequencies. *Proc. IEEE*, **62**, 33–36, 1974.